

Stony Brook University



OFFICIAL COPY

The official electronic file of this thesis or dissertation is maintained by the University Libraries on behalf of The Graduate School at Stony Brook University.

© All Rights Reserved by Author.

**Simulation of Electron Beam
Dynamics in the 22 MeV Accelerator
for a Coherent Electron Cooling Proof
of Principle Experiment**

A Thesis Presented

by

Justin Owen

to

The Graduate School

in Partial Fulfillment of the Requirements

for the Degree of

Master of Arts

in

Physics

Stony Brook University

December 2013

Stony Brook University

The Graduate School

Justin Owen

We, the thesis committee for the above candidate for the Master of Arts degree, hereby recommend acceptance of this thesis.

Vladimir Litvinenko – Thesis Advisor
Professor, Department of Physics and Astronomy

Thomas Hemmick – Chairperson of Defense
Professor, Department of Physics and Astronomy

Maria Victoria Fernandez-Serra
Professor, Department of Physics and Astronomy

This thesis is accepted by the Graduate School.

Charles Taber
Dean of the Graduate School

Abstract of the Thesis

**Simulation of Electron Beam Dynamics in the
22 MeV Accelerator for a Coherent Electron
Cooling Proof of Principle Experiment**

by

Justin Owen

Master of Arts

in

Physics

Stony Brook University

2013

Coherent electron cooling (CeC) offers a potential new method of cooling hadron beams in colliders such as the Relativistic Heavy Ion Collider (RHIC) or the future electron ion collider eRHIC. A 22 MeV linear accelerator is currently being built as part of a proof of principle experiment for CeC at Brookhaven National Laboratory (BNL). In this thesis we present a simulation of electron beam dynamics including space charge in the 22 MeV CeC proof of principle experiment using the program ASTRA (A Space charge TRacking Algorithm).

Contents

List of Figures	vi
List of Tables	viii
Acknowledgements	ix
1 Introduction	1
2 CeC Proof of Principle Experiment	3
2.1 Accelerating Structures	4
2.1.1 112 MHz Gun	4
2.1.2 500 MHz Bunching Cavities	5
2.1.3 704 MHz Cavity	6
2.2 Magnets	7
2.2.1 Solenoids	8
2.2.2 Quadrupoles	11
2.2.3 Dipoles	13
2.2.4 Helical Undulators	14
2.3 CeC Beam Parameter Requirements	15
3 Simulating With ASTRA	17
3.1 Initial Bunch Characteristics	18
3.2 Accelerator Components	18
3.3 Space Charge Calculations	19
3.4 Problems with ASTRA	20
4 Results	24
4.1 Initial Beam Settings	24
4.2 Cavity and Magnet Settings	25
4.3 The Beam in the 2 MeV Section	29
4.4 The Beam in The 22 MeV Section	34

4.5 Conclusion	38
--------------------------	----

List of Figures

1.1	FEL based coherent electron cooling	2
2.1	The economic version of FEL based CeC.	3
2.2	The 22 MeV linac injector for the CeC proof of principle experiment	4
2.3	The 112 MHz SRF gun where the electron bunch is generated.	5
2.4	The two 500 MHz bunching cavities on the left in place next to the 112 MHz gun.	6
2.5	The 704 MHz cavity (pink) shown inside its liquid helium vessel.	7
2.6	The gun solenoid (orange) around the beam pipe at the end of the 112 MHz gun	8
2.7	The solenoids used in the 2 MeV section of the 22 MeV linac.	9
2.8	The beam particles moving through the solenoid rotate inward.	10
2.9	A quadrupole used for 22 MeV electron beam transport. . . .	11
2.10	The two common dipole types, sector (left) and rectangular (right) with the beam path shown in red.	13
2.11	A 3D drawing of a dipole used in the 22 MeV linac.	14
2.12	A 3D drawing of a helical undulator used in the CeC experiment.	15
3.1	Histograms of the momentum distribution at 0.6 m.	21
3.2	Histograms of the momentum distribution of the beam after passing through a dipole.	22
3.3	Beam profile after passing through a dipole.	23
4.1	The beam profile 0.73 m from the cathode.	25
4.2	The E_z profiles used for calculating the electric fields of the cavities.	26
4.3	The B_z profiles used for calculating the magnetic fields of the solenoids.	27
4.4	The transverse beam size leading up to the 704 MHz cavity. .	29
4.5	The transverse bunch emittance leading up to the 704 MHz cavity.	30
4.6	The bunch length leading up to the 704 MHz cavity.	30

4.7	The evolution of the longitudinal beam profile along the 2 MeV section.	31
4.8	The beam profile 0.63 m before the 704 MHz cavity.	32
4.9	The longitudinal phase space characteristics of the beam 0.63 m before the 704 MHz cavity.	33
4.10	The beam profile 0.17 m after the 704 MHz cavity exit.	34
4.11	The beam profile 0.45 m before entering the undulator solenoids.	35
4.12	The beam profile midway through the undulator solenoids.	36
4.13	The beam profile as it moves into the beam dump.	37

List of Tables

2.1	The beam requirements throughout the CeC experiment. . . .	16
4.1	The values used to generate the initial particle distribution. . .	25
4.2	The values used in the cavity settings.	25
4.3	The values used in the solenoid settings.	28
4.4	The values used in the quadrupole settings.	28
4.5	The values used in the quadrupole settings.	28

Acknowledgements

The person I am most indebted to for help with this thesis is Dr. Igor Pinayev who acted as my unofficial advisor. Without his constant oversight of my work I would not have learned nearly as much. He was always there to answer my questions and had entertaining stories to lighten the day. I would like to thank my advisor, Dr. Vladimir Litvinenko, for funding my work and overseeing my thesis progress. His encouragement made this thesis progress more smoothly than I could have hoped. I also would like to thank Dr. Yue Hao for introducing me to the accelerator physics group at Brookhaven National Laboratory. Had I not been introduced to him during my first semester at Stony Brook, I don't think I would have ended up working in accelerator physics.

Surviving graduate school takes more than just great professors. I would like to thank Jocelyn Cheung for sticking it out up here in New York with me. Her need for adventure led to many enjoyable trips around Long Island and New York City. Finally, I would like to thank my friend Stephen Rowe for helping me proofread my thesis and listening to all my complaining. Without Jocelyn and Stephen graduate school would have been very different.

Chapter 1

Introduction

A 22 MeV linear accelerator (linac) is currently being built at Brookhaven National Laboratory as part of a proof of principle experiment for coherent electron cooling (CeC). Simulations of the electron bunches moving through the 22 MeV CeC linac including space charge need to be performed for further verification of how the linac will work. In this thesis we present an overview of the CeC experiment and simulations of an electron bunch traveling through the 22 MeV linac using the program ASTRA (A Space charge TRacking Algorithm).

Coherent electron cooling (CeC) is a high bandwidth form of stochastic cooling first proposed in the 1980's before the technology existed. Fortunately, advances in free electron laser (FEL) and energy recovery linac (ERL) technology make it possible to realize this idea today.

The basic idea behind CeC is to co-propagate a bunch of electrons along with the hadron bunch. These electrons will then form clouds around individual hadrons to screen the hadron charge. These electron clouds are then passed through a FEL structure where through FEL amplification their density is increased. The hadrons with the beam's energy are then recombined on top of their electron clouds so that they feel no pull from them. However, hadrons of energy greater or less than the energy of the hadron beam will be in front of the electron cloud or behind it. These hadrons will be pulled on by the cloud and experience an energy change towards the energy of the hadron beam. CeC leads to a net reduction in the energy spread of the hadron bunches.

Hadron beams in colliders do not have strong energy loss mechanisms that lead to a natural way of reducing the spread of their energy and emittances (emittance is proportional to the area in phase space occupied by the beam). Current high-energy proton colliders have no control over beam emittances at the collision energy. This means they must use beams as they are, which is

not always optimal for the luminosity of a collider.

Luminosity is a major figure of merit for a collider. It provides a metric for the productivity of a specific branch of physics in the collider. For a round beam common in hadron colliders, the luminosity is:

$$L = f_c \frac{N_1 N_2}{4\pi\beta^*\epsilon} h\left(\frac{\sigma_s}{\beta^*}\right),$$

where β^* is the transverse beta function at the collision point, ϵ is the transverse emittance, σ_s is the bunch length, N_1 and N_2 are the number of particles in each bunch, f_c is the frequency of collisions, and $h \leq 1$ is a function accounting for a phenomenon known as the hourglass effect.

The hourglass effect:

$$h(x) = \frac{\sqrt{\pi}}{x} e^{1/x^2} \operatorname{erfc}(1/x),$$

occurs when the bunch length becomes larger than β^* . The beta function will grow parabolically as a function of distance from the interaction point which causes the beam size to increase. Longitudinal cooling offers potential reduction in β^* and an increase in the collider's luminosity [1].

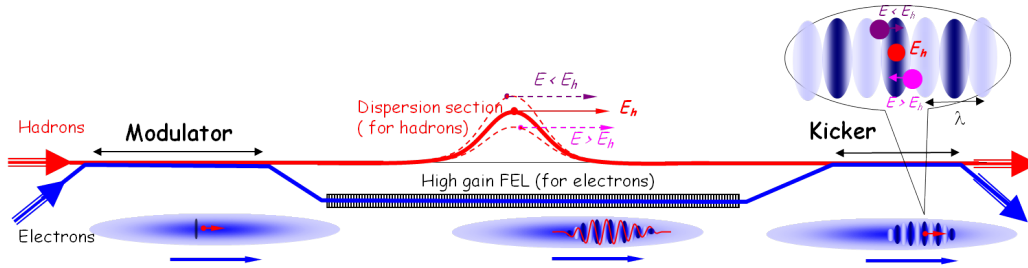


Figure 1.1: FEL based coherent electron cooling

Chapter 2

CeC Proof of Principle Experiment

The CeC proof of principle experiment is intended to experimentally verify that coherent electron cooling can be accomplished. It seeks to cool 40 GeV/nucleon Au ions with 22 MeV electrons. Due to budget constraints a more economical version of CeC shown in figure 2.1 is being used. There will be no separate dispersion section for the hadrons. This means that the hadrons will also travel through the FEL structure. This setup requires matching of the group velocity of the amplified density distortion in the FEL with the hadron velocity.

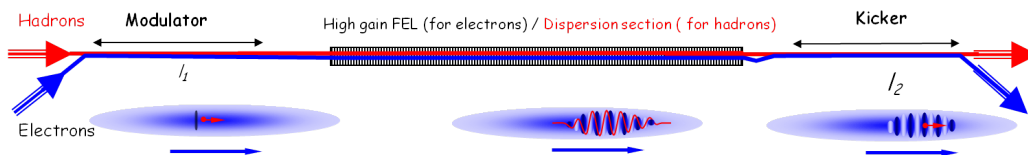


Figure 2.1: The economic version of FEL based CeC.

A 22 MeV injector is currently under construction for this experiment. It consists of two main sections: the 2 MeV gun (up to the 704 MHz cavity) and the 22 MeV section (everything after the 704 MHz cavity). The full configuration is expected to be completed by 2015. A picture of what the linac will look like is shown in figure 2.2.

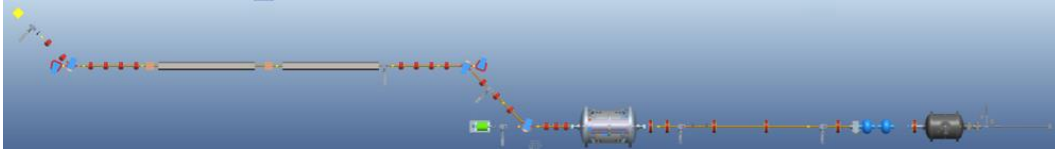


Figure 2.2: The 22 MeV linac injector for the CeC proof of principle experiment

2.1 Accelerating Structures

Superconducting radio frequency (SRF) cavities are the basic accelerating structures used in the 22 MeV linac. Each cavity has a specific resonant frequency at which electromagnetic fields are generated inside. Electromagnetic fields are fed by an RF generator which feeds electromagnetic power into these cavities. Charged particles then pass through the center of the cavity and receive energy from the electromagnetic fields that have built up inside. There are different cavity modes. The transverse magnetic (TM) field mode has magnetic fields transverse to the direction of charged particle propagation and an electric field in the direction of propagation. These modes supply acceleration to the particles. The other mode is the transverse electric (TE) field mode. This mode has electric fields transverse to the direction of propagation and provide no acceleration to the particles.

2.1.1 112 MHz Gun

The 112 MHz gun is where the electron bunch is generated; see figure 2.3. A cathode at the beginning of the gun has a laser shined on it to generate electrons. The electrons coming off the cathode are then accelerated to 2 MeV through the 0.3 m long gap [2].

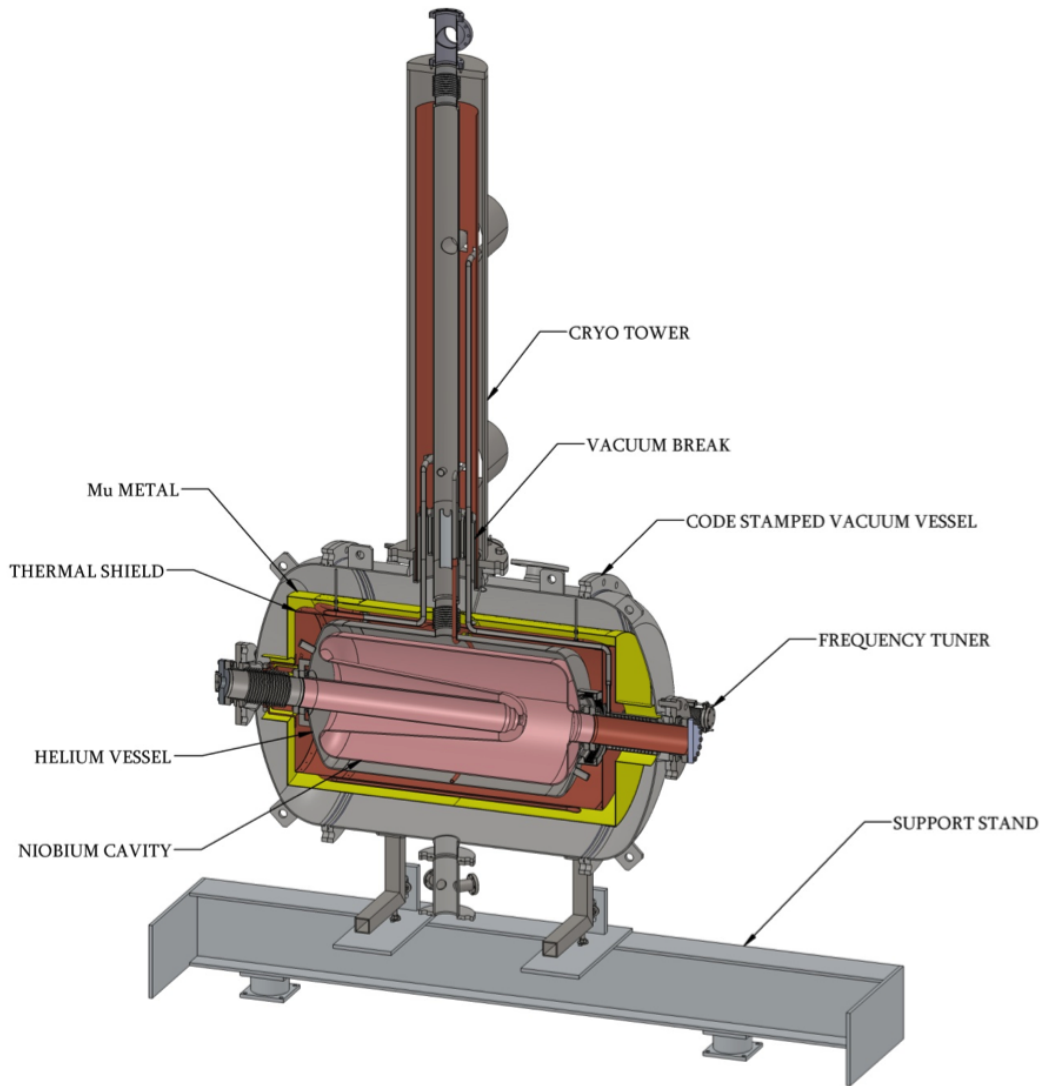


Figure 2.3: The 112 MHz SRF gun where the electron bunch is generated.

2.1.2 500 MHz Bunching Cavities

The two 500 MHz cavities will provide an energy chirp for the ballistic compression of the electron beam. Compression of the electron beam occurs in the drift space between the 500 MHz and 704 MHz cavities. Two cavities are necessary instead of one in order to get enough of an energy chirp. The bunching cavities are shown in figure 2.4 and are each 0.596 m long [2].

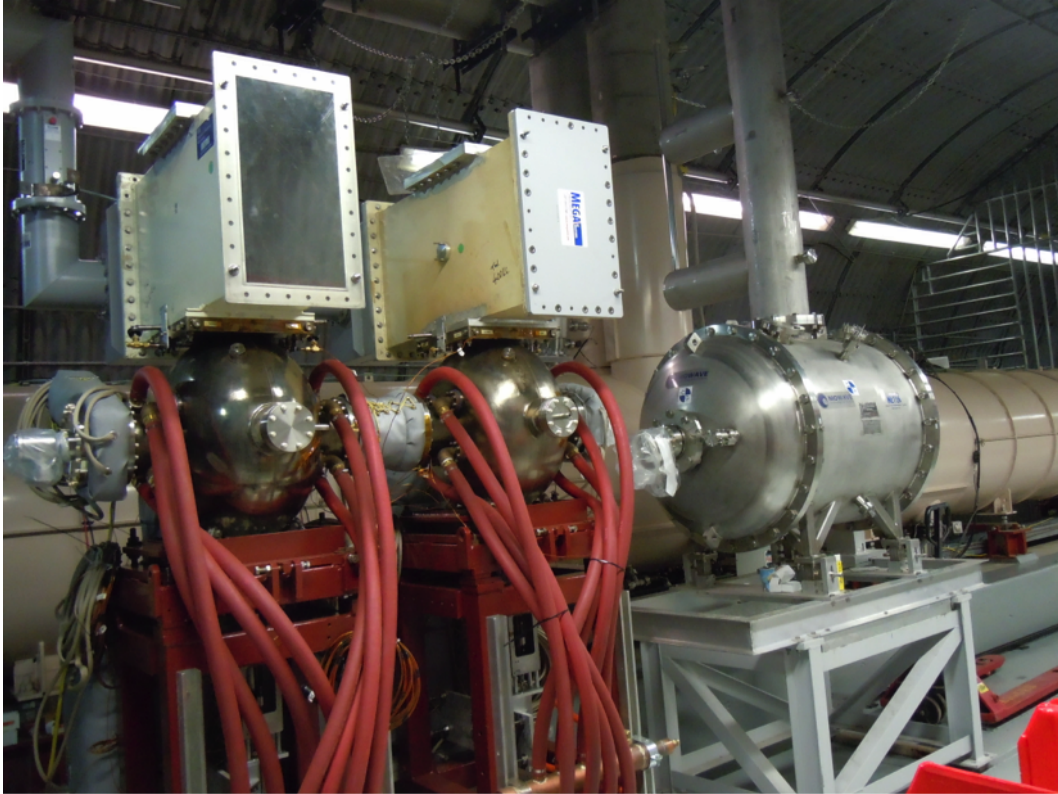


Figure 2.4: The two 500 MHz bunching cavities on the left in place next to the 112 MHz gun.

2.1.3 704 MHz Cavity

The 704 MHz cavity is 2.128 m long and accelerates the bunch to its final energy of 22 MeV. The cavity is superconducting and operates at 2 K. It is being developed by Niowave. The cavity is shown in figure 2.5 [2].

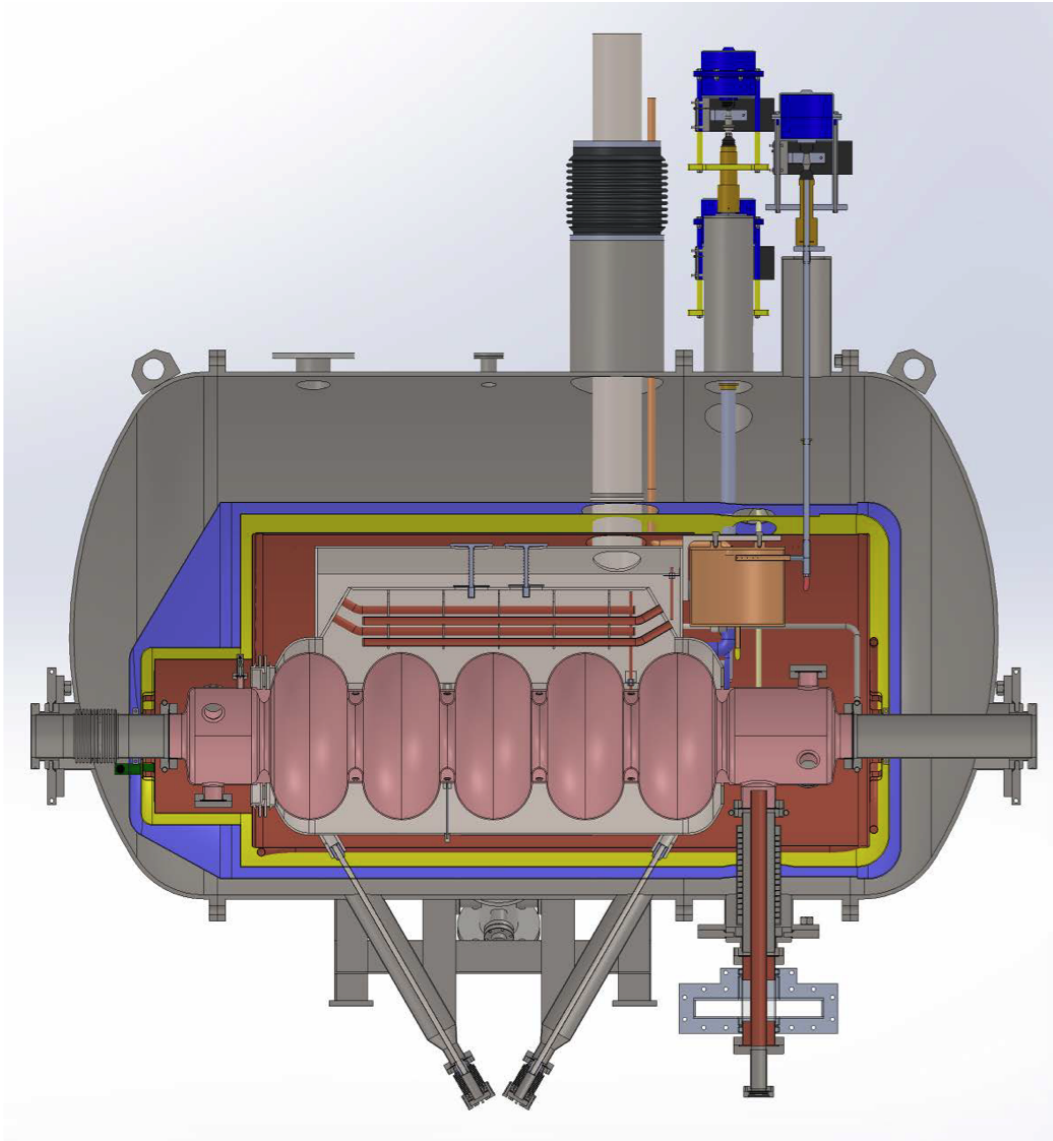


Figure 2.5: The 704 MHz cavity (pink) shown inside its liquid helium vessel.

2.2 Magnets

The magnets of an accelerator are pivotal to its operation. While cavities provide acceleration, magnets provide steering and focusing. The magnets used are solenoids, quadrupoles, and dipoles.

2.2.1 Solenoids

Solenoids provide focusing at low energies in accelerators and are the only magnets used up to the entrance of the 704 MHz cavity in the 22 MeV linac. The beam pipe is 10.16 cm in diameter and the solenoids are used to keep the bunch diameter below the diameter of the beam pipe. If the diameter of the bunch goes beyond the beam pipe diameter electrons will be lost and the beam current will drop. The vacuum pipe can also be damaged.

All the solenoids are the same except the one right outside of the 112 MHz gun (gun solenoid). The gun solenoid can be seen in figure 2.6 and the other solenoids can be seen in figure 2.7 [2].

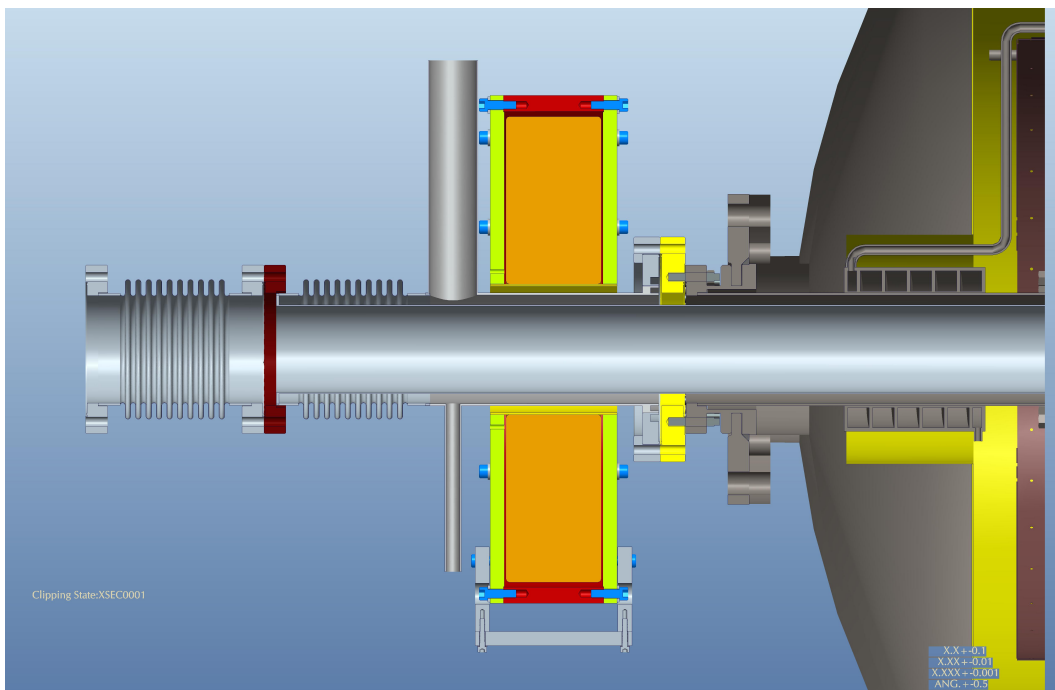


Figure 2.6: The gun solenoid (orange) around the beam pipe at the end of the 112 MHz gun

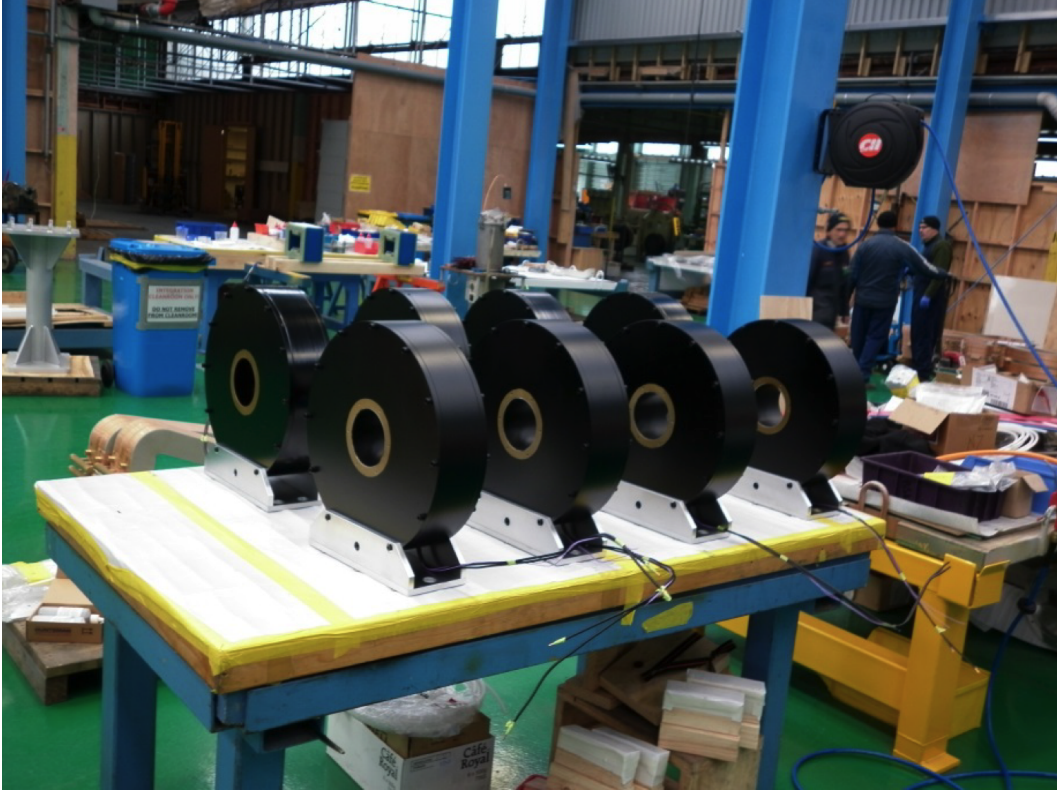


Figure 2.7: The solenoids used in the 2 MeV section of the 22 MeV linac.

Here we present a simple model of solenoid focusing [3]. Assume that the magnetic field along the axis of the solenoid is B_0 inside the solenoid and 0 outside. The field off the axis of a solenoid can be expressed as:

$$B_z(z, r) = B_z(z, 0) - \frac{r^2}{4}B_z''(z, 0) + \frac{r^4}{64}B_z^{(4)}(z, 0) + \dots$$

$$B_r(z, r) = -\frac{r}{2}B_z'(z, 0) + \frac{r^3}{16}B_z'''(z, 0) + \dots$$

Keeping terms only up to first order in r , we can represent the z component of the magnetic field using step functions as:

$$B_z(z, r) = B_0[\theta(z) - \theta(z - L)],$$

where L is the length of the solenoid. The radial magnetic field is then:

$$B_r = -\frac{r}{2}B_0[\delta(z) - \delta(z - L)].$$

An electron a distance r_0 from the z axis will experience a force $-ev_z B_r(z)$ at the entrance to the solenoid, giving:

$$\gamma m \frac{dv_\theta}{dt} = \gamma m v_z \frac{dv_\theta}{dz} = -ev_z B_r(z) = -\frac{r}{2} B_0 [\delta(z) - \delta(z - L)].$$

Integrating this and rearranging terms yields:

$$v_\theta = \frac{eB_0 r_0}{2\gamma m}.$$

As the particle moves into the solenoid, the centripetal force balances out the Lorentz force in the radial direction yielding:

$$\frac{\gamma m v_\theta^2}{R} = eB_z v_\theta.$$

The radius of curvature is then:

$$R = \frac{\gamma m v_\theta}{eB_0} = \frac{r_0}{2}.$$

Particles will rotate in a circle that has a radius equal to half the distance they are from the z -axis as can be seen in figure 2.8.

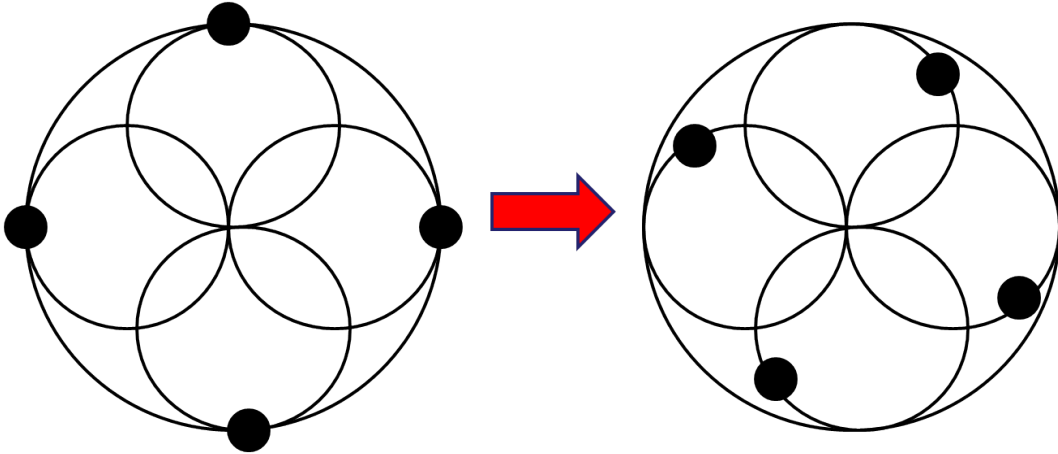


Figure 2.8: The beam particles moving through the solenoid rotate inward.

2.2.2 Quadrupoles

Quadrupoles are used for beam focusing when energies are on the order of 10 MeV and above. They provide focusing in one direction and defocusing in the other, e.g. focusing in x and defocusing in y . Aside from the dipoles, all focusing after the 704 MHz cavity is done with 0.157 m long quadrupoles like the one shown in figure 2.9 [2].

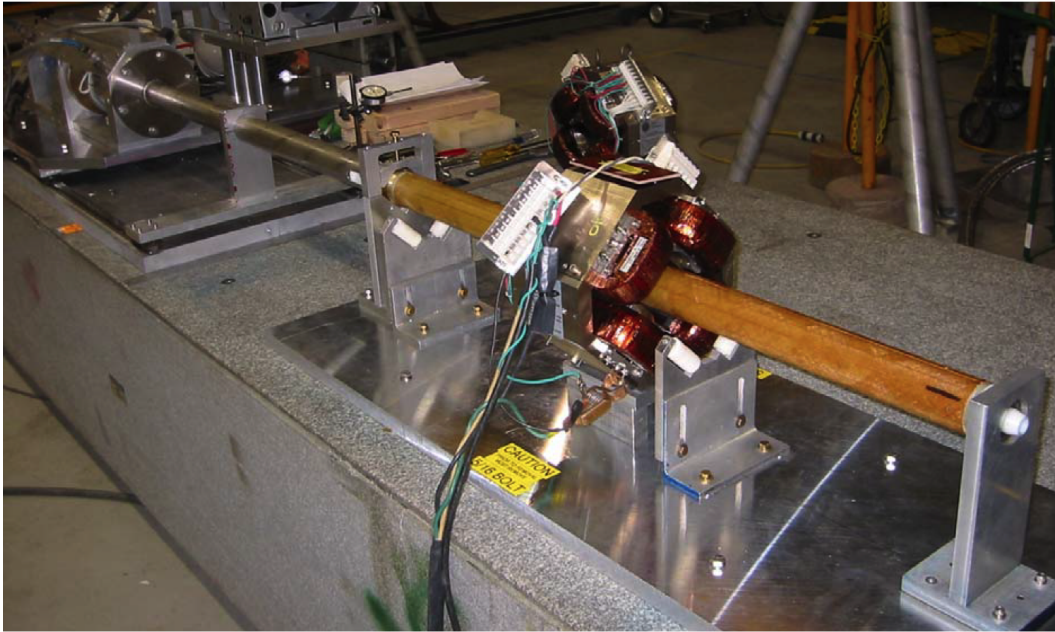


Figure 2.9: A quadrupole used for 22 MeV electron beam transport.

The transverse motion of a particle moving through a quadrupole can be explained starting with Hill's equation:

$$\frac{d^2y}{dz^2} + Ky = 0,$$

where $K = \frac{e}{p} \frac{\partial B_z}{\partial y}$ [4]. If we assume K is constant, this is the equation for a simple harmonic oscillator with solutions:

$$y(z) = \begin{cases} a \cos(\sqrt{K}z + b) & \text{if } K > 0, \\ az + b & \text{if } K = 0, \\ a \cosh(\sqrt{-K}z + b) & \text{if } K < 0, \end{cases}$$

where a and b are determined by initial conditions. We can create a transfer

matrix formalism like the ray transfer matrix formalism in optics. We represent the phase space variables for y in vector form as:

$$\mathbf{y}(z) = \begin{pmatrix} y(z) \\ y'(z) \end{pmatrix},$$

and the matrix equation is:

$$\mathbf{y}(z) = M(z|z_0)\mathbf{y}(z_0).$$

Let $l = z - z_0$, $a = 1$, and $b = 0$, then the transfer matrix $M(z|z_0)$ can be expressed as:

$$M(z|z_0) = \begin{cases} \begin{pmatrix} \cos(\sqrt{K}l) & \frac{1}{\sqrt{K}} \sin(\sqrt{K}l) \\ -\sqrt{K} \sin(\sqrt{K}l) & \cos(\sqrt{K}l) \end{pmatrix} & \text{if } K > 0, \\ \begin{pmatrix} 1 & l \\ 0 & 1 \end{pmatrix} & \text{if } K = 0, \\ \begin{pmatrix} \cosh(\sqrt{|K|}l) & \frac{1}{\sqrt{|K|}} \sinh(\sqrt{|K|}l) \\ \sqrt{|K|} \sinh(\sqrt{|K|}l) & \cosh(\sqrt{|K|}l) \end{pmatrix} & \text{if } K < 0. \end{cases}$$

We show that the form for $M(z|z_0)$ is correct by multiplying out the equation $\mathbf{y}(z) = M(z|z_0)\mathbf{y}(z_0)$ for $K > 0$ (focusing).

$$\begin{aligned} & \begin{pmatrix} \cos(\sqrt{K}l) & \frac{1}{\sqrt{K}} \sin(\sqrt{K}l) \\ -\sqrt{K} \sin(\sqrt{K}l) & \cos(\sqrt{K}l) \end{pmatrix} \begin{pmatrix} y(z_0) \\ y'(z_0) \end{pmatrix} = \\ & \begin{pmatrix} \cos(\sqrt{K}l) \cos(\sqrt{K}z_0) + \sin(\sqrt{K}l) \sin(\sqrt{K}z_0) \\ -\sqrt{K} \sin(\sqrt{K}l) \cos(\sqrt{K}z_0) - \sqrt{K} \cos(\sqrt{K}l) \sin(\sqrt{K}z_0) \end{pmatrix} = \\ & \begin{pmatrix} \cos(\sqrt{K}z) \\ -\sqrt{K} \sin(\sqrt{K}z) \end{pmatrix} = \begin{pmatrix} y(z) \\ y'(z) \end{pmatrix} \end{aligned}$$

In the limit $l \rightarrow 0$ we get the thin lens approximation:

$$M(z|z_0) = \begin{pmatrix} 1 & 0 \\ -\frac{1}{f} & 1 \end{pmatrix},$$

which is the exact same form as the thin lens ray transfer matrix from optics. Here the focal length f is:

$$f = \lim_{l \rightarrow 0} -\frac{1}{|K|l}.$$

2.2.3 Dipoles

There is a dogleg after the 704 MHz cavity. Dipoles are used to steer the beam through the dogleg. There are two main types of dipoles, sector dipoles and rectangular dipoles. Sector dipoles focus in the bending plane. This effect can be seen as geometric. Particles moving into the dipole with a transverse offset from the design path will either have a longer or shorter path through the magnet and will correspondingly be bent more or less by the magnetic fields leading to a focusing effect.

Rectangular dipoles will have no geometric focusing in the bending plane since all particles have the same path length through the magnet. However, there is vertical focusing caused by the fringe fields. Fringe fields are the fields along the edge of the dipole [5].

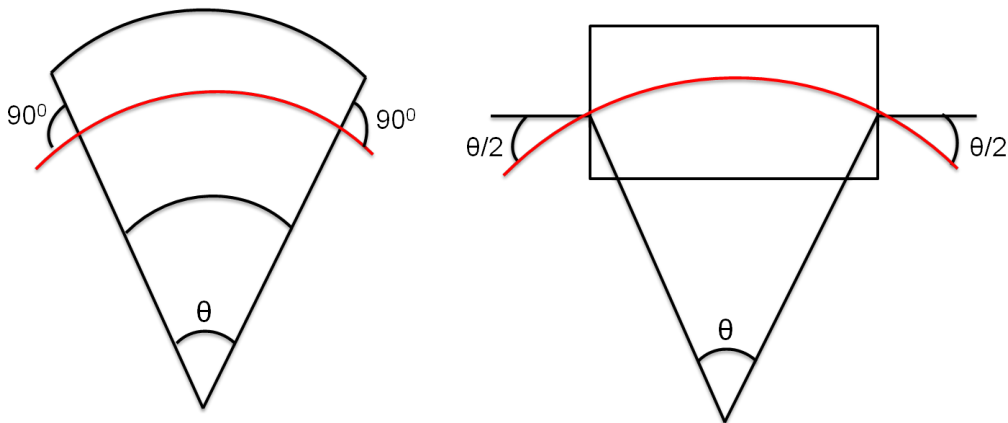


Figure 2.10: The two common dipole types, sector (left) and rectangular (right) with the beam path shown in red.

We want a magnet that focuses in both horizontal and vertical directions. The angle of entrance for a sector dipole is 0° with respect to a line normal to the entrance and this dipole has horizontal focusing. The angle of entrance for a rectangular dipole is $\theta/2$ and this dipole has vertical focusing. The chevron dipole used has an entrance angle of $\theta/4$ halfway between a sector dipole and rectangular dipole leading to equal parts fringe field vertical focusing and geometric bending plane focusing. A drawing of the dipole is in figure 2.11.

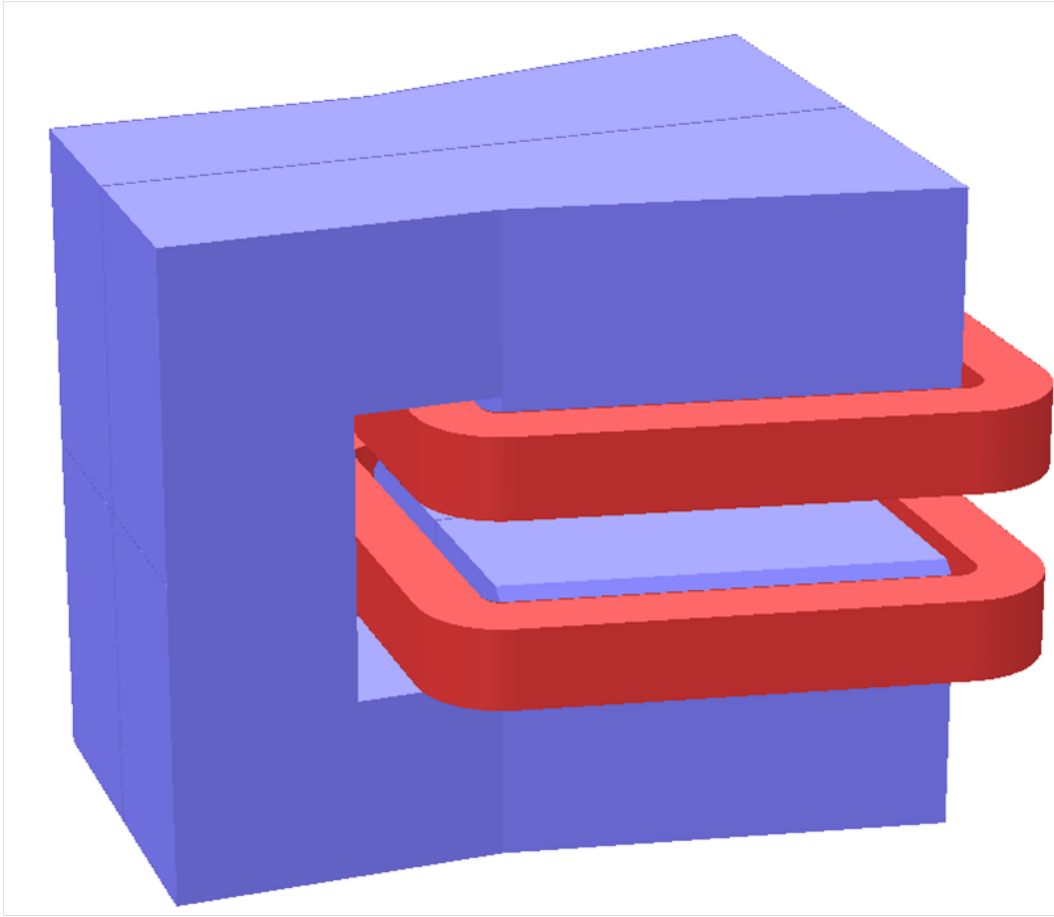


Figure 2.11: A 3D drawing of a dipole used in the 22 MeV linac.

2.2.4 Helical Undulators

Helical undulators are a series of magnets built to cause electrons to fly in a helical path. This helical path leads to the electrons producing spontaneous radiation which is essential to the FEL amplification in CeC. There are three 2.5m long helical undulators like the one pictured in figure 2.12.

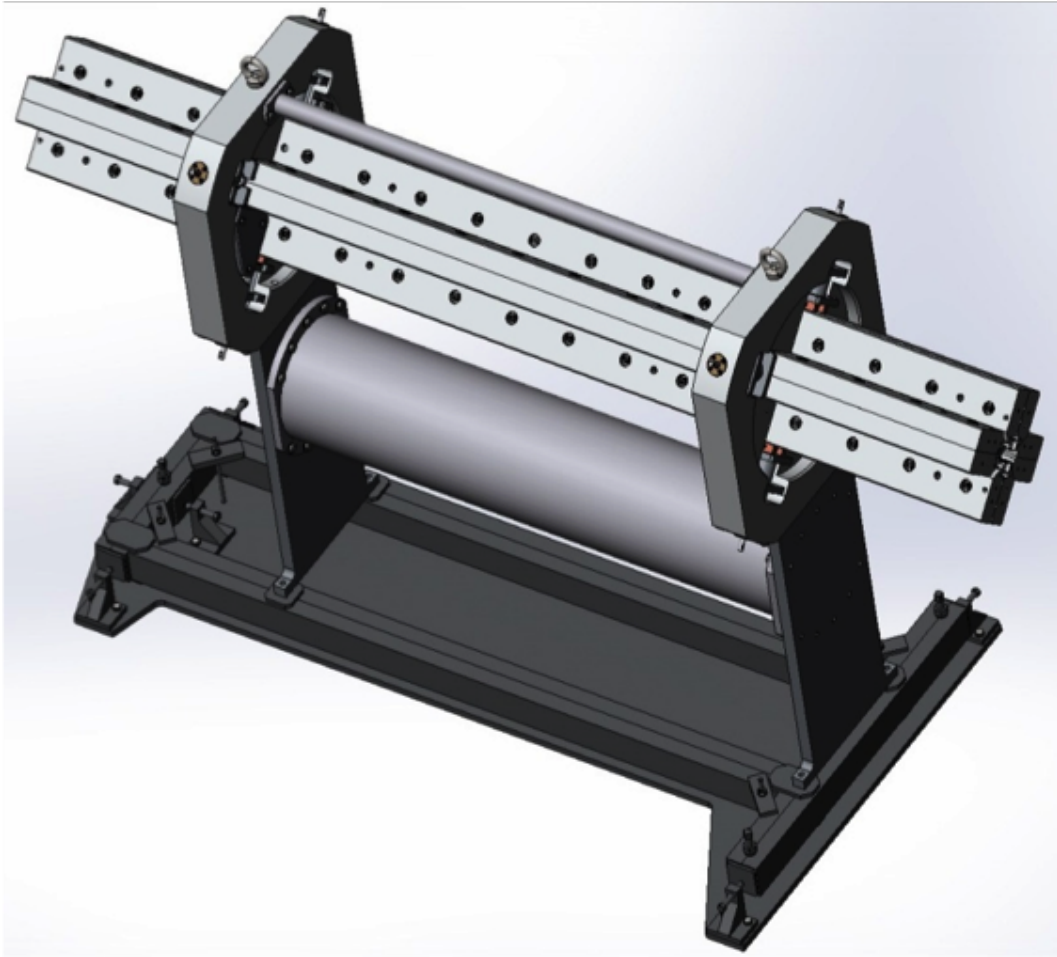


Figure 2.12: A 3D drawing of a helical undulator used in the CeC experiment.

2.3 CeC Beam Parameter Requirements

The beam requirements are listed in table 2.1.

Parameter	Requirement
Emittance [$\pi mrad \cdot mm$]	5
2 MeV Section Beam Stay Clear Size [mm]	101.6
Quadrupole Beam Stay Clear Size [mm]	50.8
Undulator Beam Stay Clear Size [mm]	32

Table 2.1: The beam requirements throughout the CeC experiment.

Chapter 3

Simulating With ASTRA

In this section we discuss how ASTRA works. When running simulations it is important to understand the limitations of the software. Unlike many of the other particle tracking programs available, such as ELEGANT, ASTRA accounts for space charge. Space charge is the charge that a particle in the electron bunch will experience from its neighbors. It is important for low energy tracking. At ultra-relativistic energies, magnetic forces compensate electric forces. For an azimuthally symmetric beam with uniform density in cylindrical coordinates, in the laboratory frame we have:

$$\begin{aligned}\nabla \cdot \mathbf{E} &= \frac{1}{\epsilon_0} \rho_0 \\ \nabla \times \mathbf{B} &= \mu_0 \rho_0 \mathbf{v}.\end{aligned}$$

Using Gauss's law we get: $E_r = \frac{1}{2\epsilon_0} \rho_0 r$. Using Ampere's law we get: $B_\phi = \frac{1}{2} \mu_0 \rho_0 v r$. We see that the Lorentz force is:

$$F_r = e(E_r - vB_\phi) = eE_r \left(1 - \frac{v^2}{c^2}\right) = \frac{1}{\gamma^2} eE_r.$$

The space charge forces are scaling as $\frac{1}{\gamma^2}$, so as the beam becomes ultra-relativistic, F_r becomes 0.

When accounting for space charge, compressing the bunch transversely and longitudinally is similar to squeezing a balloon. It will expand in the unsqueezed direction. Therefore, excessive bunching will lead to transverse expansion and excessive transverse focusing leads to the bunch lengthening. Using ASTRA allows us to find a balance between longitudinal compression and transverse focusing while accounting for space charge.

ASTRA does have some disadvantages. The main disadvantage for our

simulations is that there is no built in feature for helical undulators in ASTRA. To get around this limitation we represent the helical undulators with long solenoids. Another disadvantage is that, unlike MAFIA, ASTRA doesn't account for interactions between bunches and geometries. This means that the particles do not interact with the boundaries of the accelerator components.

3.1 Initial Bunch Characteristics

ASTRA allows the user to specify the initial bunch characteristics in six dimensional phase space (x, y, z, p_x, p_y, p_z) using a generator file. For our purposes, a radial symmetric distribution was chosen for x and y . A Gaussian distribution was chosen for $p_x, p_y,$ and p_z . The distribution in z was chosen to be a plateau or square wave shape with a rise time of $40ps$.

When specifying the number of particles in a bunch it is important to realize ASTRA works with macro particles. Each macro particle can be thought of as a ball of electrons, where no electrons inside a macro particle interact with each other. The number of macro particles in the bunch and the total charge of the bunch of macro particles is specified by the user. The number of electrons in each macro particle is $N_e = Q/(N_m e)$. While it is possible to make each macro particle have a single electron, it is not recommended since the calculation time scales with the number of particles.

3.2 Accelerator Components

ASTRA uses a global coordinate system when specifying the locations of accelerator components. The fields of the cavities and solenoids are derived from a user defined table of values for the field strengths in the longitudinal (z) direction along their axis of symmetry. Our simulations use data tables of measurements of the magnetic fields of the solenoids and the electric fields of the cavities used in the accelerator. Once a table of values is specified, the field strength can be adjusted by specifying the maximum value of the magnetic field for each solenoid and the maximum electric field strength for each cavity. The values in the table are rescaled to these specified maximums. For cavities, the relative phase between the wave in the cavity and the bunch can be specified and the frequency of the cavity needs to be specified.

The field of the solenoids are derived using a field expansion of \mathbf{B} :

$$B_z(z, r) = B_z(z, 0) - \frac{r^2}{4} B_z''(z, 0) + \frac{r^4}{64} B_z^{(4)}(z, 0) + \dots,$$

$$B_r(z, r) = -\frac{r}{2}B'_z(z, 0) + \frac{r^3}{16}B'''_z(z, 0) + \dots$$

The transverse magnetic (TM) fields of the cavities are expanded as:

$$E_z(z, r) = \left[E_z(z, 0) - \frac{r^2}{4} \left(E''_z(z, 0) + \frac{\omega^2}{c^2} E_z(z, 0) \right) \right] \sin(\omega t),$$

$$E_r(z, r) = \left[-\frac{r}{2}E'_z(z, 0) + \frac{r^3}{16} \left(E'''_z(z, 0) + \frac{\omega^2}{c^2} E'_z(z, 0) \right) \right] \sin(\omega t),$$

$$B_\phi(z, r) = \left[\frac{r}{2}E_z(z, 0) - \frac{r^3}{16} \left(E''_z(z, 0) + \frac{\omega^2}{c^2} E_z(z, 0) \right) \right] \frac{\omega}{c^2} \sin(\omega t).$$

A transverse electric (TE) field can be expanded as:

$$B_z(z, r) = \left[B_z(z, 0) - \frac{r^2}{4} \left(B''_z(z, 0) + \frac{\omega^2}{c^2} B_z(z, 0) \right) \right] \cos(\omega t),$$

$$E_r(z, r) = \left[-\frac{r}{2}B'_z(z, 0) + \frac{r^3}{16} \left(B'''_z(z, 0) + \frac{\omega^2}{c^2} B'_z(z, 0) \right) \right] \cos(\omega t),$$

$$E_\phi(z, r) = \left[\frac{r}{2}B_z(z, 0) - \frac{r^3}{16} \left(B''_z(z, 0) + \frac{\omega^2}{c^2} B_z(z, 0) \right) \right] \omega \sin(\omega t).$$

Dipoles are created by specifying the entrance and exit faces of each dipole. ASTRA automatically calculates the magnetic field if the bending radius for the bunch is specified. The quadrupoles are characterized by specifying their length and focal strength.

3.3 Space Charge Calculations

For calculation of space charge, a grid containing the bunch is Lorentz transformed into the average rest system of the bunch. This makes the motion of the particles non relativistic. A 4th order Runge-Kutta method is used for time steps.

The default static field calculation method is used in our simulations. This method creates a cylinder centered on the z -axis in cylindrical coordinates (z ,

r, ϕ) containing the bunch and grids this cylinder using rings in the r coordinate, and slices in the z direction. Calculations are then done numerically by integrating over the rings and assuming a constant charge density inside of a ring. The field contributions of the individual rings at the centers of the grid cells are added up and transformed back into the lab frame. The field between points is calculated using cubic spline interpolation [6].

3.4 Problems with ASTRA

The 22 MeV linac has a dogleg that bends the beam at a 45° angle. Simulations using the dipole feature of ASTRA were performed. These simulations were found to have problems. As mentioned earlier, ASTRA does all calculations in the average rest frame of the beam. All calculations then assume that the particles are moving at non-relativistic speeds. If we have a z momentum of 22 MeV/c going into a 45° dipole, then the x momentum after the dipole would be:

$$p_x = (22 \text{ MeV}/c) \sin(-45^\circ) = -15.6 \text{ MeV}/c = p_z.$$

Figure 3.1 shows the histograms of the momentum in each direction of the beam in the average rest frame according to ASTRA at around 0.6 m. Figure 3.2 shows the histograms of the beam's momenta after passing through a dipole. We expect distributions centered around momentum of 0 since calculations are done in the average rest frame, but the distribution for p_x is concentrated near the momentum of $p_x = -15.9 \text{ MeV}/c$ which is near the p_x value that was calculated. ASTRA is only transforming to the average rest frame in z and is not properly transforming to the average rest frame in x and y , and produces erroneous results when tracking particles. Figure 3.3 shows the erroneous results caused by ASTRA incorrectly transforming to the average rest frame. Notice the white lines appearing.

In our model dipoles are replaced with solenoids to provide the same focusing in both planes. To prevent beam rotation each dipole solenoid will be split in half with each half having equal field strength in opposite directions.

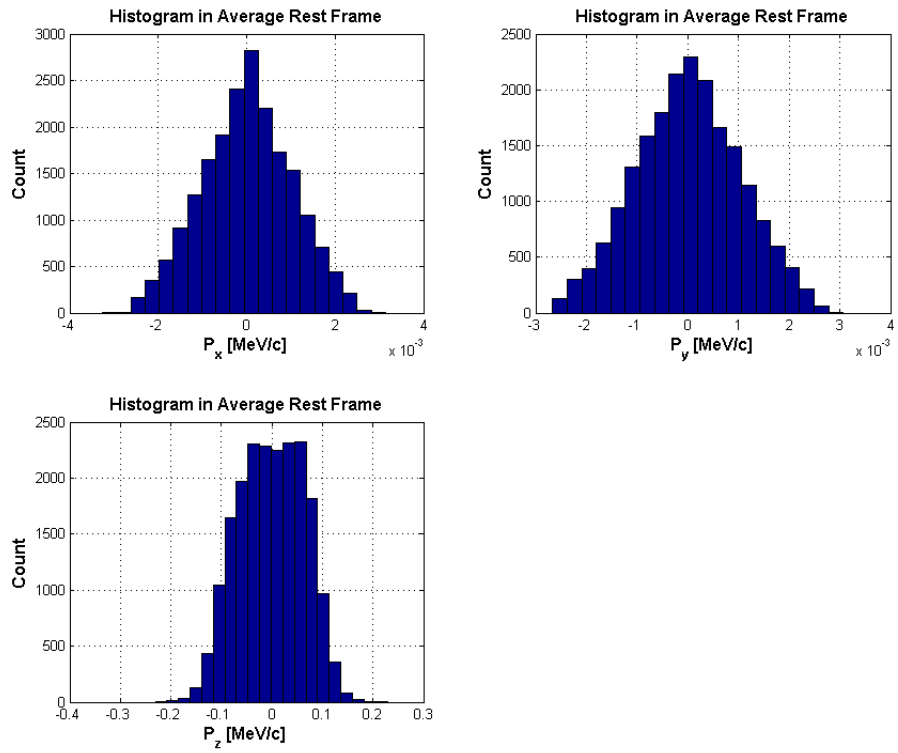


Figure 3.1: Histograms of the momentum distribution at 0.6 m.

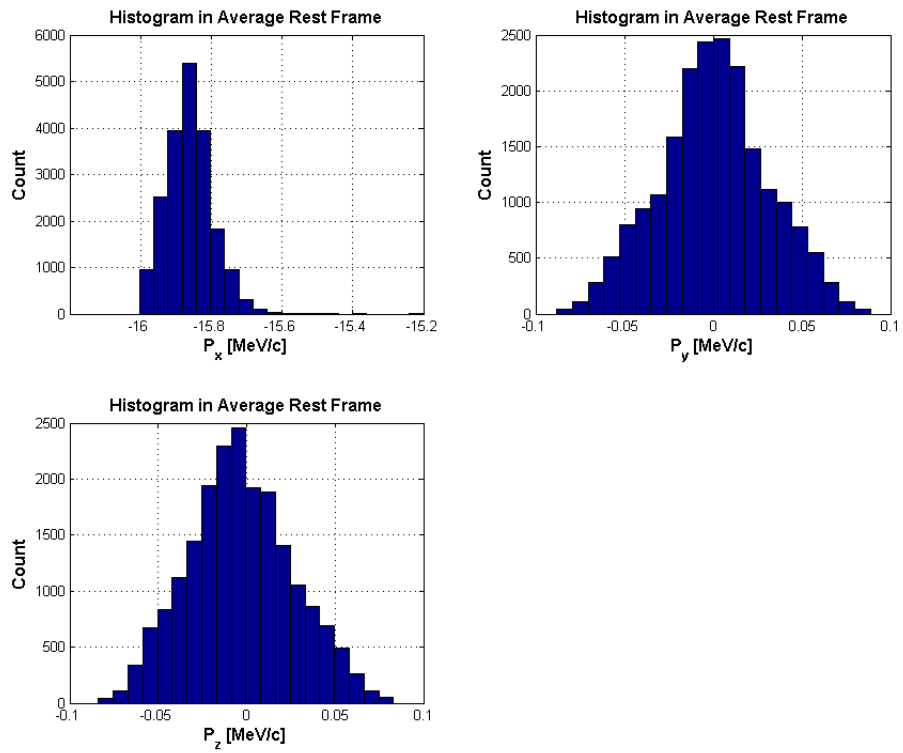


Figure 3.2: Histograms of the momentum distribution of the beam after passing through a dipole.

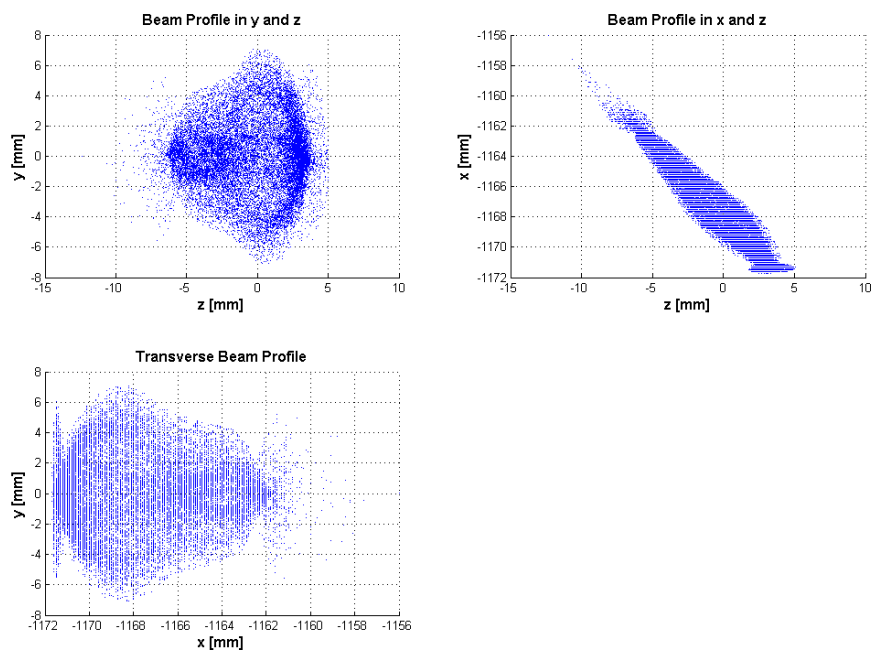


Figure 3.3: Beam profile after passing through a dipole.

Chapter 4

Results

4.1 Initial Beam Settings

The initial beam distribution uses a plateau distribution in z described by the function:

$$f(t) = \frac{1}{t_L} \frac{1}{1 + \exp\left(\frac{2}{t_r}(2|t| - t_L)\right)},$$

where t_L is the full width half maximum (FWHM) of $f(t)$ which we specify in time and t_r is the time for a line of slope $S = \frac{d}{dt}f(t)|_{\pm \frac{t_L}{2}}$ to go from 0 to the height of the plateau. The initial beam distribution in x and y is given by the flat radial function:

$$f(x, y) = \begin{cases} \frac{1}{\pi r^2} & \text{if } x^2 + y^2 \leq r^2 \\ 0 & \text{if } x^2 + y^2 > r^2 \end{cases},$$

where $\sigma_r = \frac{r}{2}$. The momentum distributions p_x , p_y , and p_z are described by the Gaussian function:

$$f(x) = \frac{1}{\sqrt{2\pi}\sigma} \exp\left(-\frac{1}{2} \frac{x^2}{\sigma^2}\right).$$

The values used in the generator file of ASTRA to create the initial particle phase space distribution are listed in table 4.1. A total bunch charge of $Q = 1.2nC$ was used. Graphs of the beam profile 0.73 m from the cathode are shown in figure 4.1.

Variable	z	p_z	x and y	p_x and p_y
Shape	Plateau	Gaussian	Radial	Gaussian
Characteristic	$t_L = 150ps, t_r = 40ps$	$\sigma = 0.25eV/c$	$\sigma_r = 1mm$	$\sigma_\epsilon = 0mrad \cdot mm$

Table 4.1: The values used to generate the initial particle distribution.

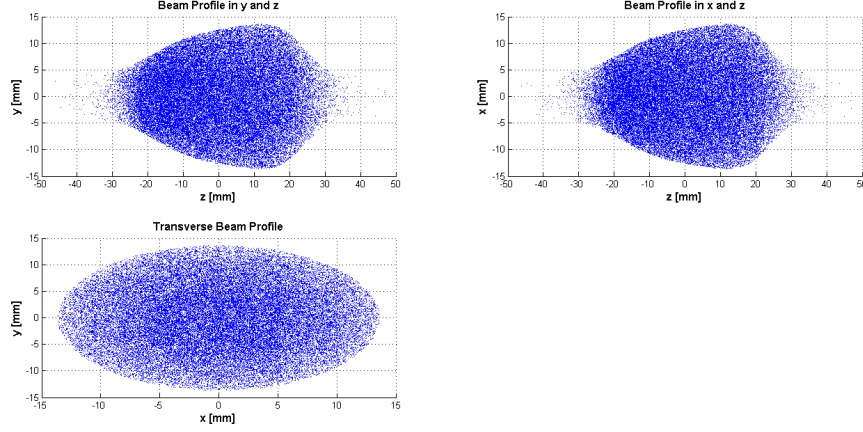


Figure 4.1: The beam profile 0.73 m from the cathode.

4.2 Cavity and Magnet Settings

ASTRA derives the electric fields of the cavities from a table of values for E_z along the z -axis. The profiles of E_z for each cavity are displayed in figure 4.2. The maximum E_z which each E_z profile is scaled around is given in table 4.2.

Cavity	112 MHz	500 MHz 1	500 MHz 2	704 MHz
Max E_z [MV/m]	22.57	1.5	1.5	37.16
Phase [deg.]	0.5	-90	-90	1.1
Length [m]	0.3	0.596	0.596	2.128

Table 4.2: The values used in the cavity settings.

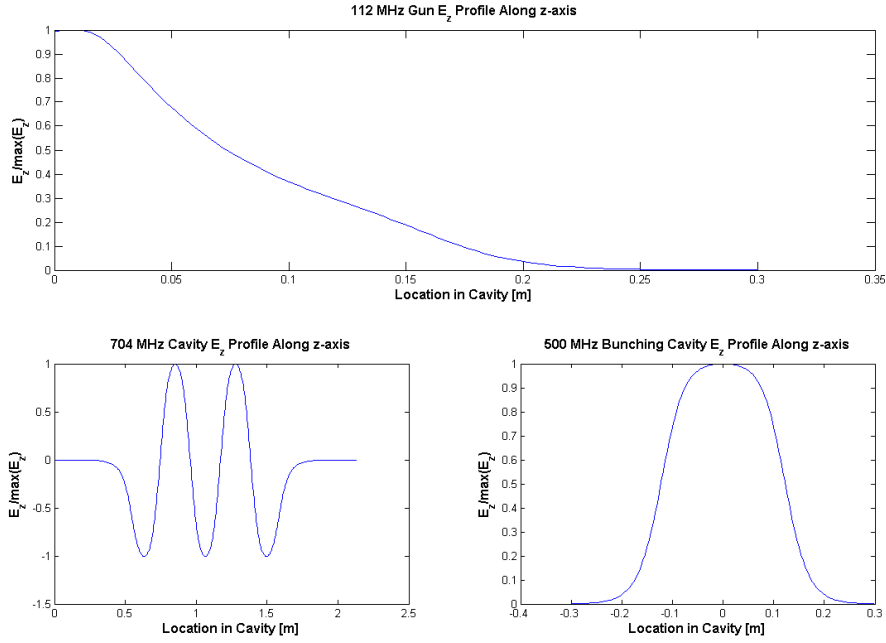


Figure 4.2: The E_z profiles used for calculating the electric fields of the cavities.

ASTRA derives the magnetic fields of the solenoids from a table of values for B_z along the z -axis. The profiles of B_z for each solenoid are displayed in figure 4.3. The dipole solenoid has a magnetic field pointing in opposite directions for each half. This is done to help counteract the rotation of the beam caused by the solenoids that would not be caused by a dipole. The maximum B_z which each B_z profile is scaled around is given in table 4.3. The focusing strengths for the quadrupoles were calculated using a program called MAD8. There values are given in tables 4.4 and 4.5.

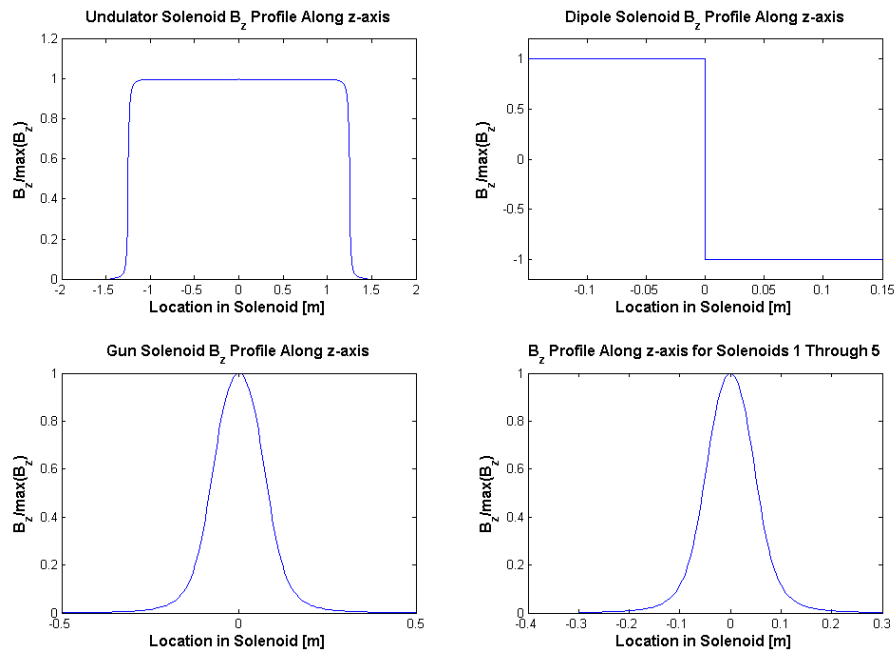


Figure 4.3: The B_z profiles used for calculating the magnetic fields of the solenoids.

Solenoid	Gun	1	2	3	4	5	Dipole 1	Dipole 2	Undulator
Max B_z [T]	0.06	0.025	0.035	0.04	0.045	0.05	0.0158	0.0158	0.1
z position [m]	0.65	3.63	6.23	8.13	9.83	10.43	14.91	18.91	21.95
Length [m]	0.3	0.2	0.2	0.2	0.2	0.2	0.3	0.3	2.9

Table 4.3: The values used in the solenoid settings.

Quadrupole	1	2	3	4	5	6	7
Focusing Strength	4.68	-15.41	15.93	16.07	-10.84	16.07	-2.10
z Position [m]	13.5	13.97	14.43	15.69	16.47	17.25	18.62

Table 4.4: The values used in the quadrupole settings.

Quadrupole	8	9	10	11	12	13	14
Focusing Strength	6.71	-7.66	3.38	3.38	-7.66	6.71	-2.1
z Position [m]	19.21	19.8	20.39	29.88	30.47	31.06	31.65

Table 4.5: The values used in the quadrupole settings.

4.3 The Beam in the 2 MeV Section

We see a gradual decrease in the bunch size after passing through each solenoid. The rms transverse bunch size in the 2 MeV section is plotted in figure 4.4. This beam size is well within the 10.16 cm beam pipe diameter. If the beam is over focused the transverse bunch size would eventually become small enough so that space charge force overcomes the focusing and causes the bunch to start growing transversely making the bunch's emittance unstable. We can see from figure 4.5 that this is not the case for our bunch and the solenoids keep the emittance stable. The emittance is also less than $5 \pi \text{mrad} \cdot \text{mm}$ as required in the design of the linac. The rms bunch length is plotted in figure 4.6. We see that after the bunch passes through the bunching cavities at around 2 m the bunch length gradually decreases indicating that the electron bunch is indeed being compressed by the bunching cavities. A similar situation of over compression can occur leading to the bunch decompressing itself.

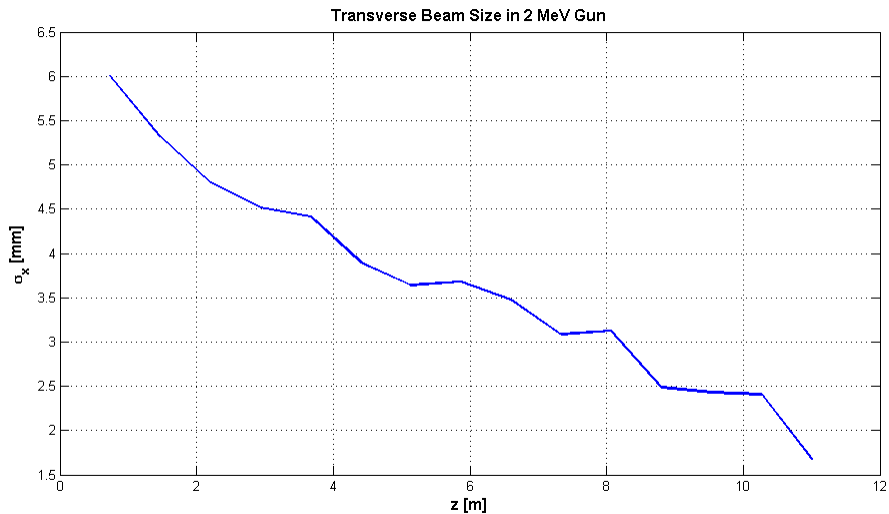


Figure 4.4: The transverse beam size leading up to the 704 MHz cavity.

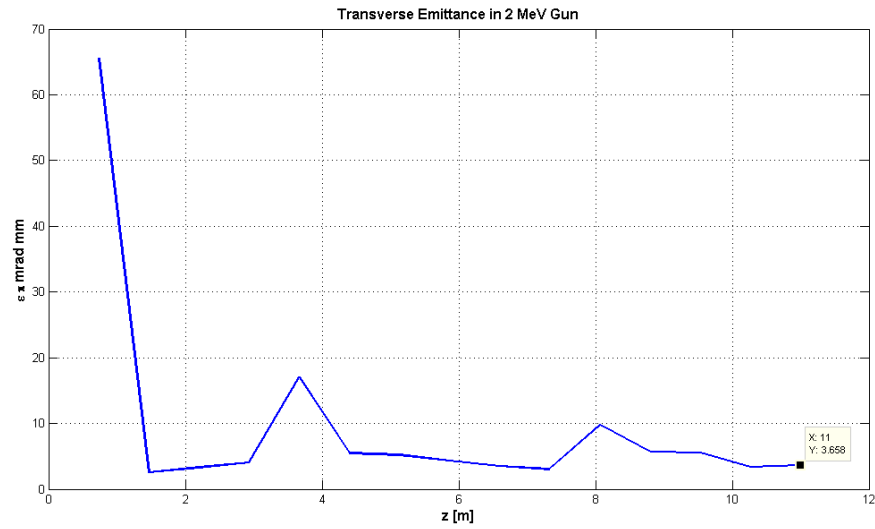


Figure 4.5: The transverse bunch emittance leading up to the 704 MHz cavity.

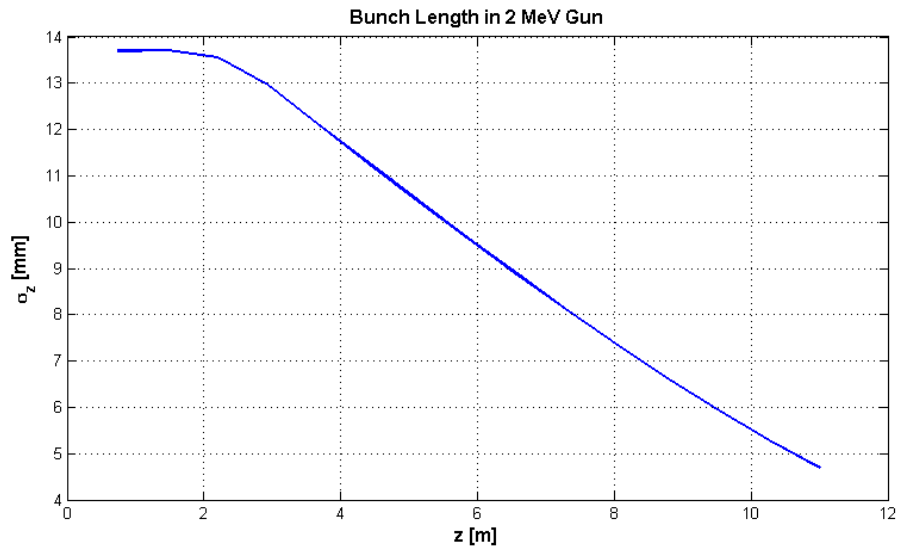


Figure 4.6: The bunch length leading up to the 704 MHz cavity.

The evolution of the beam along the 2 MeV section can be seen in figure 4.7. The ends of the beam begin to form an hourglass shape as a result of over focusing with the solenoids. The front of the beam gradually folds back on the beam. The profile of the beam 0.63 m from the 704 MHz cavity entrance can be seen in figure 4.8. The transverse beam profile in figure 4.8 is radially

symmetric as is expected with solenoid focusing. The longitudinal phase space characteristics of the beam 0.63 m from the 704 MHz cavity entrance are shown in figure 4.9. The folding of the front of the beam is causing a noticeable spike in the beam current at the front of the beam. This spike in the beam current will continue to grow as the beam is accelerated through the 704 MHz cavity. This can be seen in the momentum distribution of the beam in figure 4.9. The front of the beam is slower than the rest of the beam, so as the beam gains energy from the 704 MHz cavity the front will continue folding back, increasing the charge density and the current.

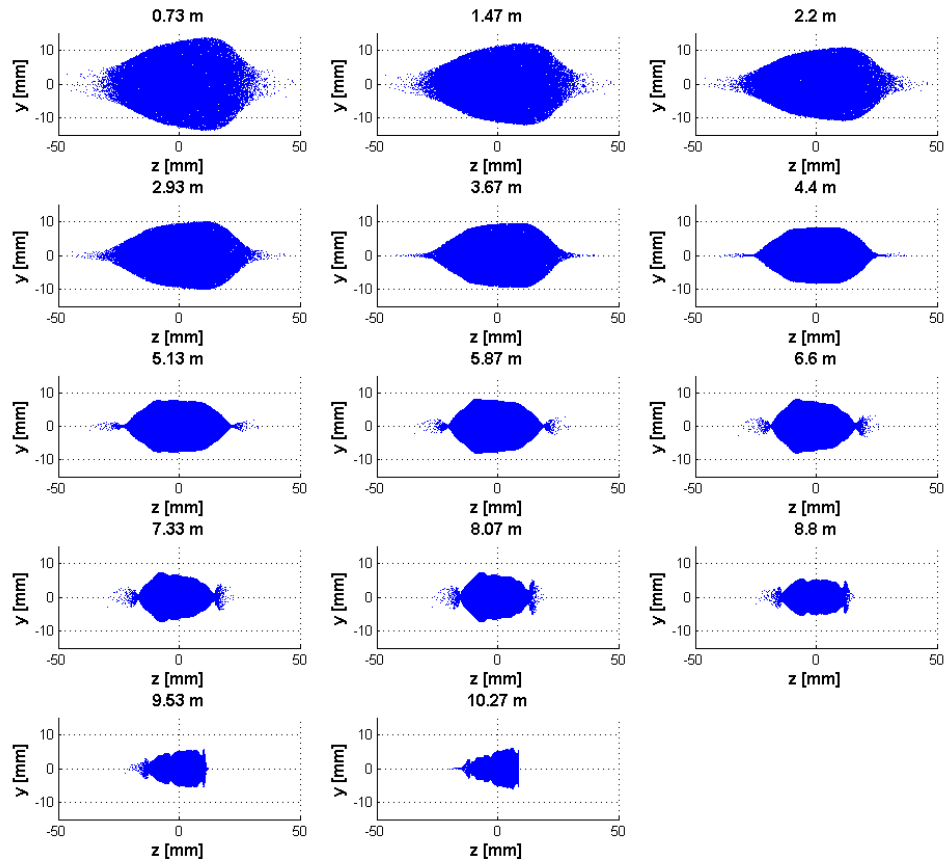


Figure 4.7: The evolution of the longitudinal beam profile along the 2 MeV section.

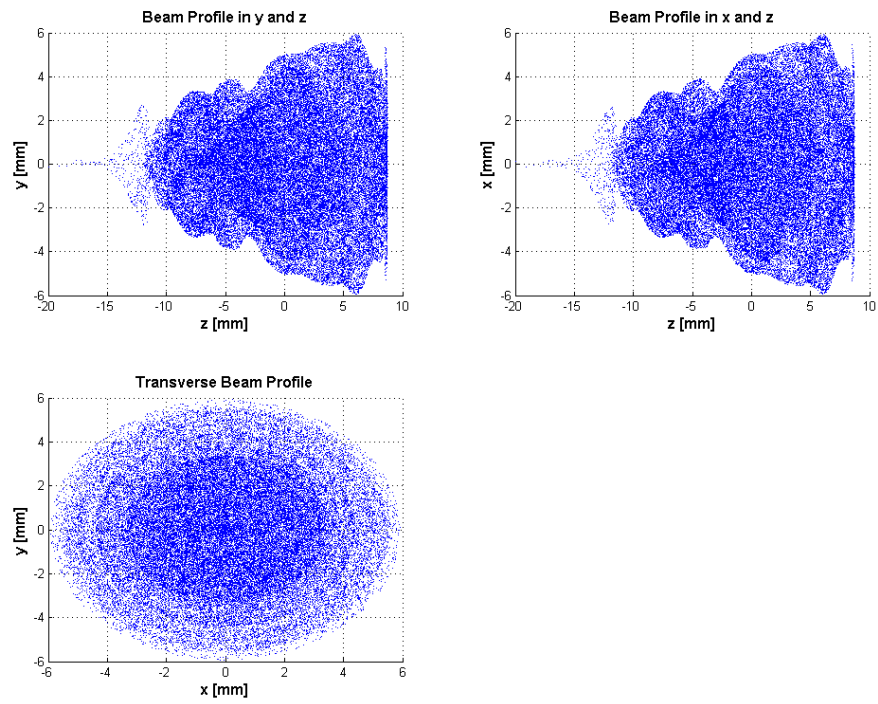


Figure 4.8: The beam profile 0.63 m before the 704 MHz cavity.

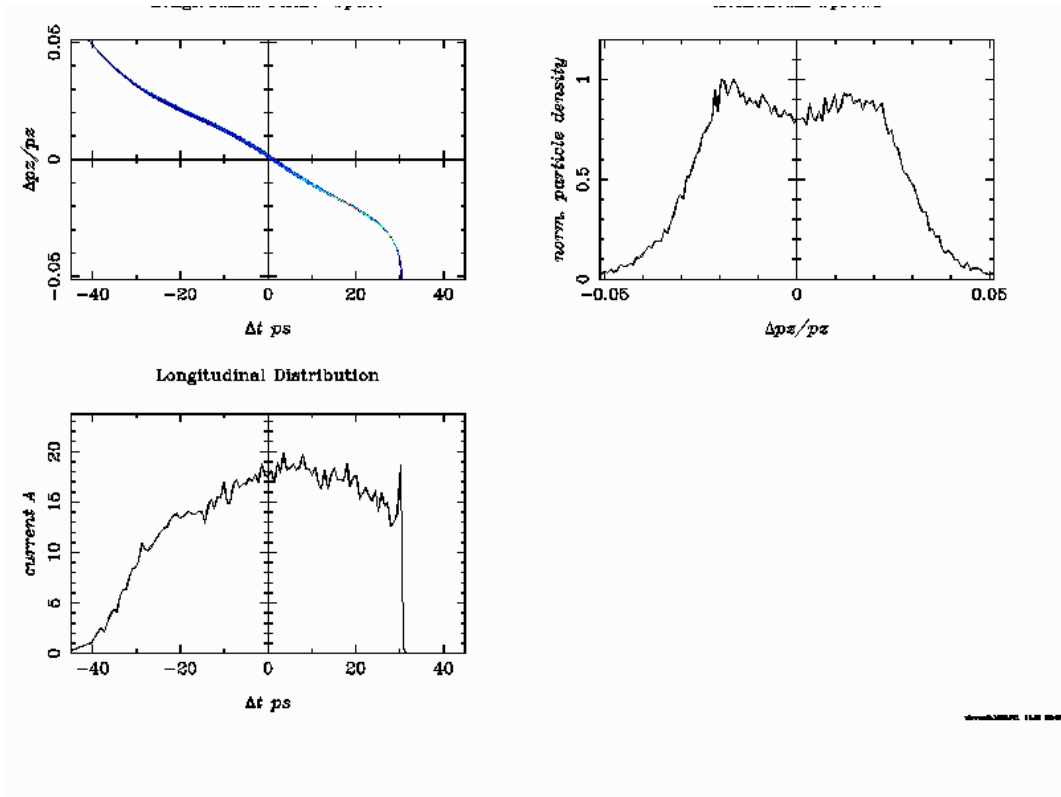


Figure 4.9: The longitudinal phase space characteristics of the beam 0.63 m before the 704 MHz cavity.

4.4 The Beam in The 22 MeV Section

After exiting the 704 MHz cavity, the beam has a axisymmetric profile as can be seen in figure 4.10. The transverse beam diameter is well within the 5.08 cm diameter of the quadrupoles. At the entrance of the undulator (figure 4.11) the beam is no longer symmetric. This is a result of the quadrupoles' focal strengths not being properly calibrated. The width of the beam is around 60 mm which exceeds the 32 mm diameter requirement for the beam while it is in the undulator.

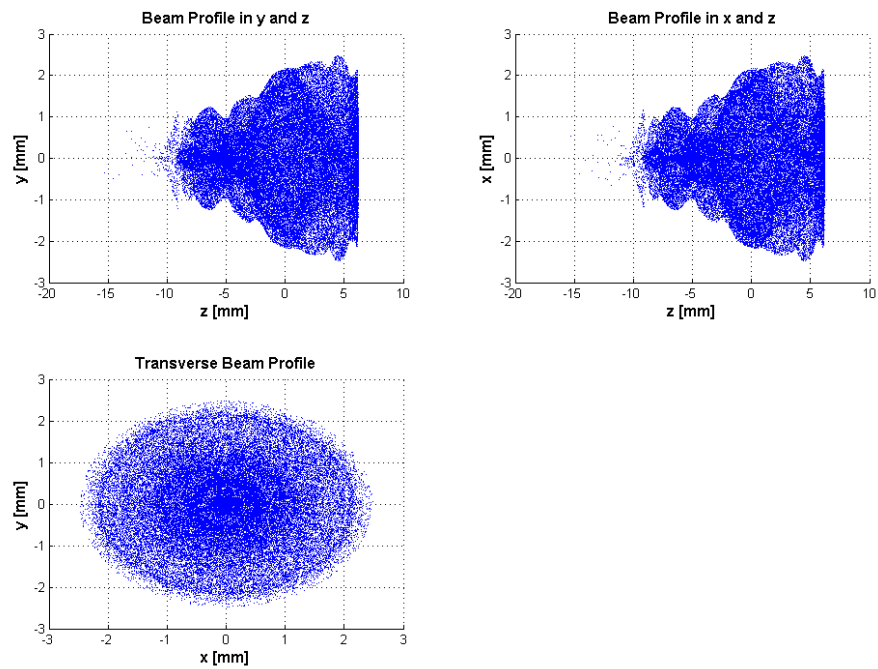


Figure 4.10: The beam profile 0.17 m after the 704 MHz cavity exit.

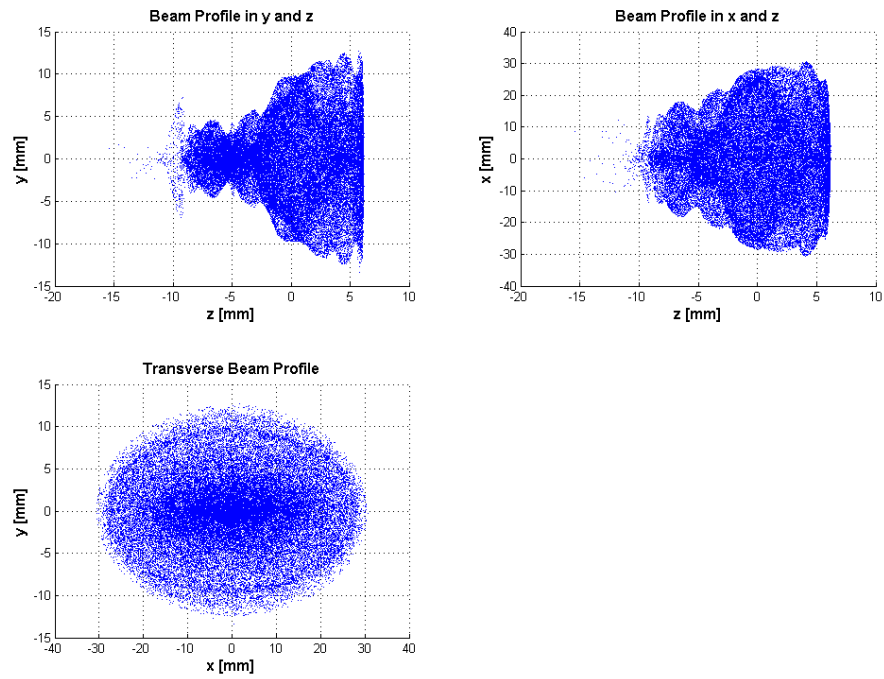


Figure 4.11: The beam profile 0.45 m before entering the undulator solenoids.

The profile of the beam in the middle of the undulators section can be seen in figure 4.12. The beam rotation caused by the solenoids is made more apparent by the elliptic transverse profile that is present at the entrance of the undulator. Figure 4.13 shows the beam profile as it moves into the beam dump.

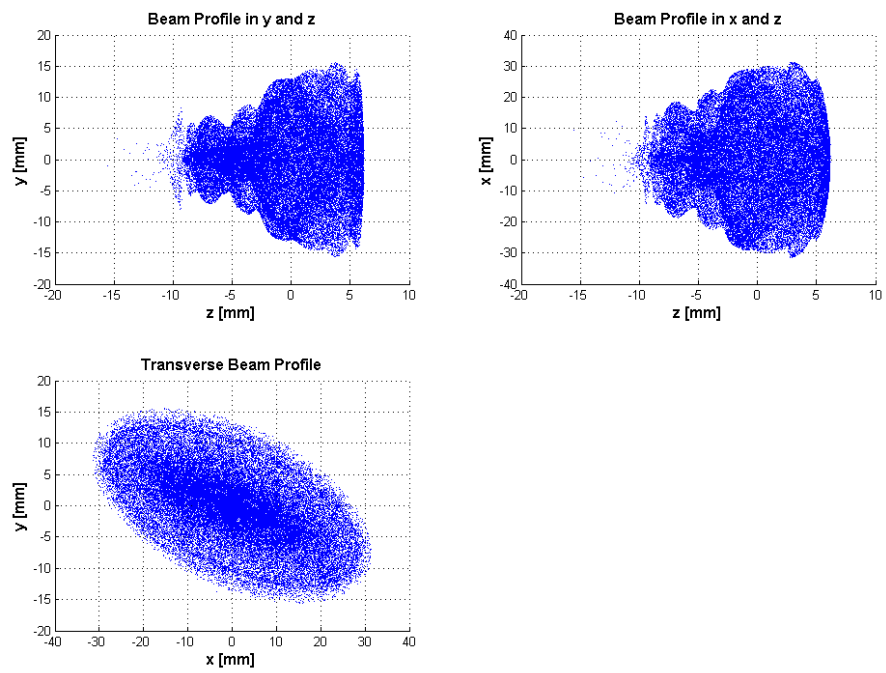


Figure 4.12: The beam profile midway through the undulator solenoids.

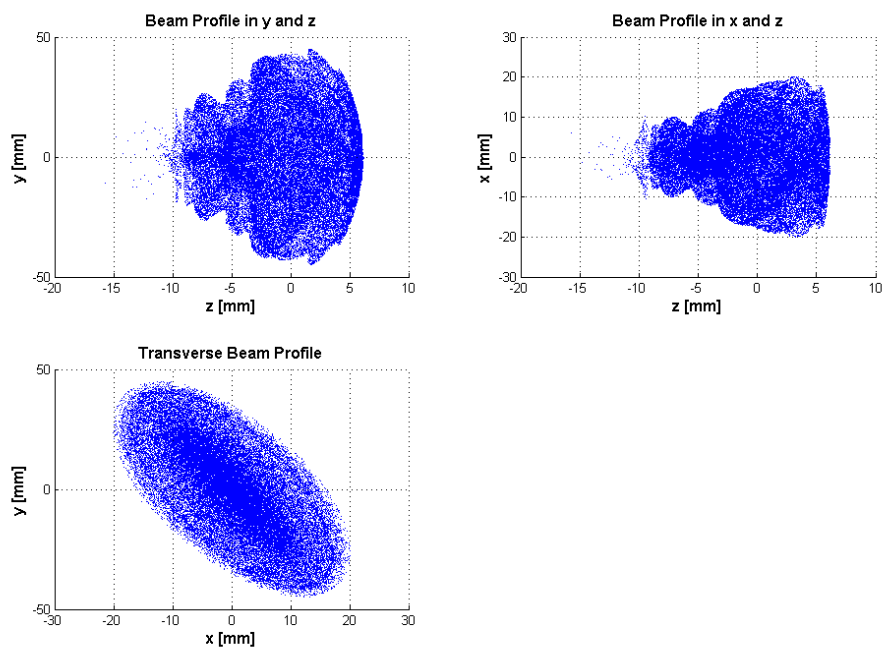


Figure 4.13: The beam profile as it moves into the beam dump.

4.5 Conclusion

Simulations of the beam with space charge were performed using ASTRA. To counteract the shortcomings of ASTRA, solenoids were used to represent the fields of dipoles and undulators. Despite these shortcomings, ASTRA provides us with a first look at the characteristics of the electron beam with space charge effects as it passes through the 22 MeV CeC linac. This is a first model of the 22 MeV linac that requires further improvements.

Further calibrations in the focal strength of the solenoids are necessary to counteract the over focusing seen in figure 4.7. The focal strengths of the quadrupoles leading into the undulators also need to be adjusted to fit beam diameter requirements given in table 2.1. The ASTRA output files at the entrance to the dipole section could be fed into a simulation using ELEGANT to get a more accurate representation of the dipole effects.

Bibliography

- [1] Vladimir Litvinenko and Yaroslav Derbenev. Free electron lasers and high-energy electron cooling. In *Proceedings of FEL 2007*, pages 268–275, 2007.
- [2] Igor Pinayev et al. Present status of coherent electron cooling proof-of-principle experiment. In *Proceedings of COOL2013*, 2013.
- [3] Vinit Kumar. Understanding the focusing of charged particle beams in a solenoid magnetic field. *American Journal of Physics*, 77(737), 2009.
- [4] S.Y. Lee. *Accelerator Physics*. World Scientific, 2004.
- [5] Helmut Wiedemann. *Particle Accelerator Physics; 3rd ed.* Springer, Berlin, 2007.
- [6] Klaus Floettmann. *ASTRA Manual V3.0*. DESY, October 2011.